A Single-Switch IPT Driver for Unipolar-Bipolar Composite Coils Achieving Misalignment Tolerance

Zhicong Huang, *Senior Member, IEEE*, Jingyu Wang, *Student Member, IEEE*, Jun Cheng, *Student Member, IEEE*, and Chi-Kwan Lee, *Senior Member, IEEE*

***Abstract*—Misalignment tolerance is a critical performance metric for inductive power transfer (IPT) systems. Various composite coil designs, such as double-D quadrature pad (DDQP), quadruple D square pad (QDSP), and rectangular solenoidal pad (RSP), have been successfully developed to generate complementary magnetic fields to mitigate this problem. However, the inclusion of two inverters often results in increased circuit components, size, and cost, which can be drawbacks for many low-to-medium power consumer applications. This letter proposes a simple single-switch IPT driver that utilizes both fundamental and second harmonics currents to energize a set of composite coils. Using RSP as an example, the unipolar coil is excited by the fundamental harmonic as usual, while the bipolar coil is driven by the second harmonic current. This approach not only reduces circuit complexity but also simplifies the control method, eliminating the need for active detection and control mechanisms. The letter details the analysis, design, simulations, and validation process of the experiment.**

***Index Terms*—Inductive Power Transfer, Single-Switch, Misalignment Tolerance, Composite Coils.**

I. INTRODUCTION

MISALIGNMENT tolerance is crucial in inductive power transfer (IPT) systems. Various magnetic coupler structures designed to mitigate the misalignment effects have been extensively studied [1]–[3]. Among these designs, combining unipolar and bipolar coils arranged orthogonally has proven effective [4]. The unipolar and bipolar coils generate or capture vertical and horizontal magnetic flux that exhibit inverse trends with misalignment, thereby ensuring stable magnetic coupling despite misalignment. Based on this principle, several magnetic couplers have been developed and deployed, such as double-D quadrature pad (DDQP) [4], quadruple D square pad (QDSP) [5], and rectangular solenoidal pad (RSP) [6].

In general, two excitation methods are commonly used for the unipolar and bipolar coils. One applies phase-reversible (0°or 180°) excitation currents depending on the misalignment conditions. Given a fixed excitation current, the bipolar coil inevitably undergoes polarity reversal (the magnetic field direction alters) across the entire misalignment range, while the unipolar coil remains unaffected, as evident in [6]. Therefore, detecting the misalignment direction and actively reversing the excitation current for the bipolar coil can reconfigure a symmetric magnetic field without polarity reversal, fully complementary to that of the unipolar coil, thereby maintaining stable magnetic coupling throughout the entire misalignment range. In [7], the unipolar and bipolar coils are independently driven, and three operating modes are utilized (unipolar coil only, bipolar coil only, and both coils) based on the misalignment conditions. To eliminate the need for detection and control, another method uses currents with a fixed 90° phase shift to excite the unipolar and bipolar coils. Magnetic field distribution can be shaped by adjusting the phase shift angle of the excitation currents [8]. Ref. [6] and [9] use excitation currents with a fixed 90° phase shift for the RSP and rectangular-double-solenoidal pad (RDSP), respectively, to achieve an even magnetic field distribution across the misalignment range, thereby realizing control-free misalignment tolerance. Building on this principle, Ref. [10] extends the misalignment-tolerant coils to an array configuration for dynamic IPT. Although these studies eliminate the need for detection and control, two inverters for the separate excitation currents are still needed. To reduce the component count of inverters, Ref. [11] proposes employing two single-switch inverters to independently drive the decoupled transmitter coils. However, this approach still requires the use of two inverters.

It is noteworthy that both excitation methods for the unipolar and bipolar coils necessitate at least two inverters, leading to more power switches and greater circuit complexity. To reduce the inverter count, this letter proposes a single-switch IPT driver that utilizes both fundamental and second harmonics to drive the unipolar-bipolar composite coils, enhancing misalignment tolerance. As revealed in [12], the single-switch IPT driver inherently has a significant second harmonic that can be used for power transfer, a component typically ignored in prior designs. By leveraging this, one coil is excited by the fundamental harmonic as usual, while the other is driven by extracting the significant inherent second harmonic from the single-switch IPT driver, eliminating the need for additional inverters. The proposed method is analyzed with a detailed

Manuscript received 25 Jul. 2025, revised 25 Aug. 2025, accepted 22 Sep. 2025. This work was supported by the National Natural Science Foundation of China under Grant 52577198 and the Guangzhou Municipal Science and Technology Bureau under Grant 2025A04J7064. *(Corresponding author: Jingyu Wang.)*

Zhicong Huang, Jingyu Wang, and Jun Cheng are with the Shien-Ming Wu School of Intelligent Engineering, South China University of Technology, Guangzhou, 510006, China (e-mail: zhiconghuang@scut.edu.cn).

Chi-Kwan Lee is with the School of Electrical and Data Engineering, University of Technology Sydney, Ultimo, NSW, Australia (email: chik-wan.lee@uts.edu.au).

TABLE I
A COMPARISON OF EXCITATION METHODS FOR MISALIGNMENT TOLERANCE

References	Inverter Number	Switch Number	Detection and Active Control	Harmonic Orders of Inputs	Shoot-through Issue
[7]	2	8	Needed	Fundamental	Yes
[6]	2	8	Not Needed	Fundamental	Yes
[11]	2	2	Needed	Fundamental	Yes
Proposed	1	1	Not Needed	Fundamental and Second	No

compensation design and validated through simulations and experiments, using an RSP as an example. Compared with conventional methods, the proposed method reduces circuit complexity by requiring only a single power switch and simplifies control, as no active detection and control are needed, as summarized in Table I.

II. Proposed Single-Switch IPT Driver and Operating Principle

A. Schematics of the Proposed Single-Switch IPT Driver

The schematic of the proposed system is shown in Fig. 1. The proposed method employs a single-switch inverter topology to generate precisely regulated high-frequency AC power [13]. The load-independent characteristic guarantees that the inverter's voltage waveform (u_{L}) maintains topological invariance under varying load conditions, thereby ensuring stable outputs of harmonic components. As highlighted by the red dashed box in Fig. 1, the operating waveforms of the AC inductor L_{E} include both fundamental and second harmonic components, which have been detailed in [12]. With the parameters given in Table II, the fundamental and second-harmonic inputs are calculated as $U_{\mathrm{L},1} = 193.1$ V and $U_{\mathrm{L},2} = 129.0$ V, as also indicated in Fig. 1. Within the misalignment range, both $U_{\mathrm{L},1}$ and $U_{\mathrm{L},2}$ remain nearly constant.

TABLE II
PARAMETER DESIGN OF THE SINGLE-ENDED IPT DRIVER

Parameter	Definition	Value
f_{s}	Operating frequency	100 kHz
U_{DC}	Input DC voltage	110 V
D	Duty cycle	0.5
D_{Z}	ZVS margin	0.11

The output voltage of the single-switch IPT inverter is then processed by two independent compensation networks, which are responsible for the fudamental and second harmonics and driving the transmitter coils $L_{\mathrm{P},1}$ (the unipolar coil) and $L_{\mathrm{P},2}$ (the bipolar coil), respectively. $L_{\mathrm{P},1}$ is a rectangular coil, while $L_{\mathrm{P},2}$ is a solenoidal coil, arranged orthogonally and magnetically decoupled from each other, as depicted in the blue dashed box in Fig. 1. L_{S} is a rectangular receiver coil. The receiver coil is compensated by a dual-frequency network, which is capable of providing resonant paths for both the fundamental and second harmonics. To discern the parameters associated with these harmonics, the subscript "1" will represent the fundamental component, while the subscript "2" signifies the second-order harmonic.

B. Operation Principle

Assuming that the compensation circuits are well designed according to the above-mentioned principle, an equivalent circuit of the approach IPT driver can be illustrated by Fig. 2(a), where two transmitters are driven by AC voltage sources with different frequencies. According to Fourier transform principles, the current of the receiver can be derived as Eq. (1). Although the mutual inductance of M_{P2S} of the magnetic coupler undergoes polarity reversal as shown in Fig. 2(b), Eq. (1) can remain constant regardless of the polarity reversal issue, given that $|\omega_{\mathrm{s},1} M_{\mathrm{P1S}} I_{\mathrm{P},1}|$ and $|\omega_{\mathrm{s},2} M_{\mathrm{P2S}} I_{\mathrm{P},2}|$ can be designed to complement each other. In other words, the proposed excitation method is feasible to achieve misalignment tolerance with a single-switch IPT driver.

$$\begin{aligned} |I_{\mathrm{S}}| &= |I_{\mathrm{S},1} + I_{\mathrm{S},2}| \\ &= \sqrt{(\omega_{\mathrm{s},1} M_{\mathrm{P1S}} I_{\mathrm{P},1}/R_{\mathrm{ac}})^2 + (\omega_{\mathrm{s},2} M_{\mathrm{P2S}} I_{\mathrm{P},2}/R_{\mathrm{ac}})^2} \end{aligned} \quad (1)$$

where the R_{ac} represents the ac equivalent resistance.

III. Compensation Network Design

A. Harmonic Separation Compensation Network on Transmitter Side

To realize the equivalent circuit in Fig. 2(a), it is necessary to establish individual resonant channels for the fundamental and second harmonics. To satisfy this requirement, this paper proposes a harmonic separation compensation network, and the corresponding schematics are depicted in Fig. 3. The shaded blocks exhibit high-impedance characteristics at specific frequencies, satisfying Eq. (2) and Eq. (3).

$$\begin{cases} j\omega_{\mathrm{s},1} L_1 = \dfrac{j\omega_{\mathrm{s},1} L_{\mathrm{a}} \frac{1}{j\omega_{\mathrm{s},1} C_{\mathrm{a}}}}{j\omega_{\mathrm{s},1} L_{\mathrm{a}} + \frac{1}{j\omega_{\mathrm{s},1} C_{\mathrm{a}}}} \\ j\omega_{\mathrm{s},2} L_{\mathrm{a}} = -\dfrac{1}{j\omega_{\mathrm{s},2} C_{\mathrm{a}}} \end{cases} \quad (2)$$

$$\begin{cases} j\omega_{\mathrm{s},1} L_{\mathrm{b}} = -\dfrac{1}{j\omega_{\mathrm{s},1} C_{\mathrm{b}}} \\ \dfrac{1}{j\omega_{\mathrm{s},2} C_1} = \dfrac{j\omega_{\mathrm{s},2} L_{\mathrm{b}} \frac{1}{j\omega_{\mathrm{s},2} C_{\mathrm{b}}}}{j\omega_{\mathrm{s},2} L_{\mathrm{b}} + \frac{1}{j\omega_{\mathrm{s},2} C_{\mathrm{b}}}} \end{cases} \quad (3)$$

For the fundamental harmonic component, the compensation network of the transmitter circuit in Fig. 1 is equivalent

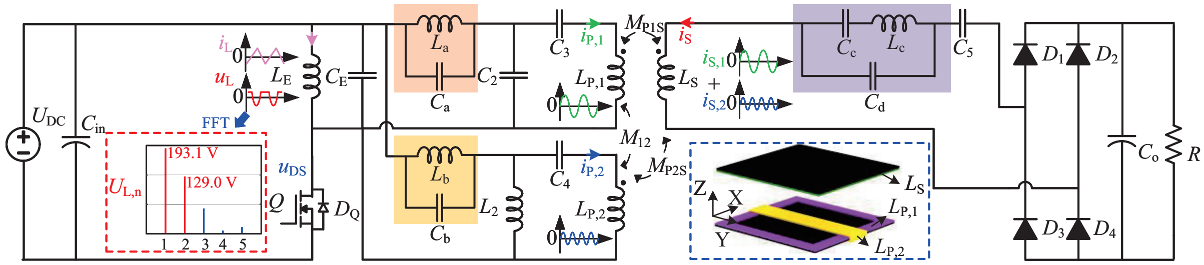

Fig. 1. The schematic of the proposed system.

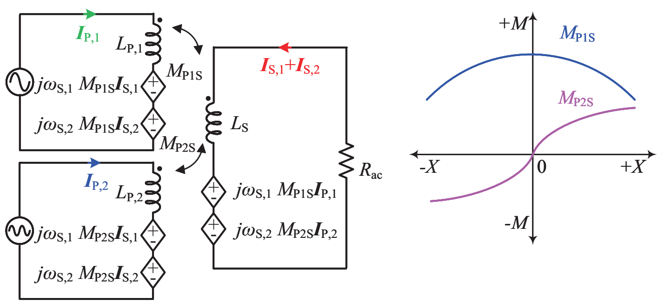

(a) Equivalent circuit. (b) Mutual inductances

Fig. 2. Equivalent circuit of the proposed system and mutual inductances of the magnetic coupler.

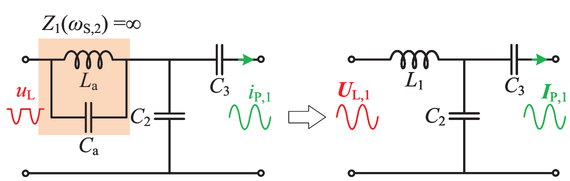

(a) Fundamental harmonic.

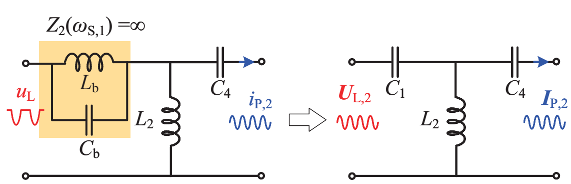

(b) Second harmonic.

Fig. 3. The harmonic separation compensation network.

to an LCL-type circuit as shown in Fig. 3(a), and it satisfies Eq. (4).

$$\begin{cases} j\omega_{s,1}L_1 = -\dfrac{1}{j\omega_{s,1}C_2} \\ j\omega_{s,1}L_1 = j\omega_{s,1}L_{P,1} + \dfrac{1}{j\omega_{s,1}C_3} \end{cases} \tag{4}$$

The excitation current of coil L_{P1} can be calculated by

$$I_{P,1} = |I_{P,1}| = \frac{|U_{L,1}|}{j\omega_{s,1}L_1}. \tag{5}$$

Similarly, the components in Fig. 3(b) comply with Eq. (6), constituting an equivalent CLC-type circuit.

$$\begin{cases} -\dfrac{1}{j\omega_{s,2}C_1} = j\omega_{s,2}L_2 \\ -j\omega_{s,2}L_2 = j\omega_{s,2}L_{P,2} + \dfrac{1}{j\omega_{s,2}C_4} \end{cases} \tag{6}$$

And the excitation current of coil L_{P2} can be calculated by

$$I_{P,2} = |I_{P,2}| = \frac{|U_{L,2}|}{j\omega_{s,2}L_2}. \tag{7}$$

B. Design of the Receiver Side and Misalignment Tolerance Analysis

As revealed by the aforementioned analysis, the receiver in the proposed circuit is exposed to electrical power at two operational frequencies, necessitating the establishment of individual resonant channels for each. The Thévenin and Norton equivalent circuits of the receiver are illustrated in Fig. 4.

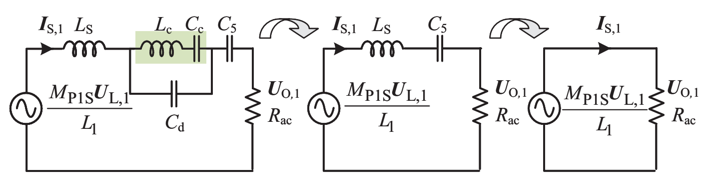

(a) Fundamental harmonic.

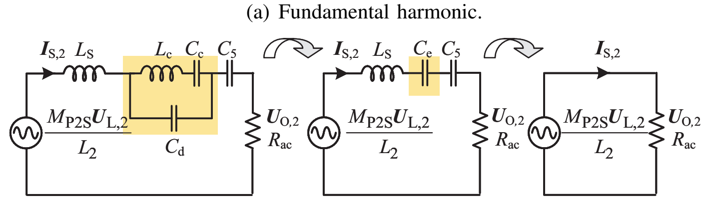

(b) Second harmonic.

Fig. 4. Equivalent circuits using Thevenin's and Norton's Theorem.

For the fundamental harmonic, as shown in Fig. 4(a), L_c and C_c satisfy Eq. (8), and the L_S is compensated by C_5.

$$\begin{cases} j\omega_{s,1}L_c = -\dfrac{1}{j\omega_{s,1}C_c} \\ j\omega_{s,1}L_S = -\dfrac{1}{j\omega_{s,1}C_5} \end{cases} \tag{8}$$

Consequently, the output voltage induced by the fundamental component is denoted by $U_{O,1}$ and can be derived as

$$U_{O,1} = |U_{O,1}| = \frac{|U_{L,1}|M_{P1S}}{L_1}. \tag{9}$$

For the second harmonic, as shown in Fig. 4(b), the network of L_c, C_c, and C_d can be regarded as a capacitor C_e, which is connected in series with C_5 to compensate L_S. The relationship satisfies the following equations.

$$\begin{cases} \dfrac{1}{j\omega_{\mathrm{s},2}C_\mathrm{e}} = \dfrac{(j\omega_{\mathrm{s},2}L_\mathrm{c} + \frac{1}{j\omega_{\mathrm{s},2}C_\mathrm{c}})\frac{1}{j\omega_{\mathrm{s},2}C_\mathrm{d}}}{j\omega_{\mathrm{s},2}L_\mathrm{c} + \frac{1}{j\omega_{\mathrm{s},2}C_\mathrm{c}} + \frac{1}{j\omega_{\mathrm{s},2}C_\mathrm{d}}} \\ j\omega_{\mathrm{s},2}L_\mathrm{S} = -\dfrac{1}{j\omega_{\mathrm{s},2}C_\mathrm{e}} - \dfrac{1}{j\omega_{\mathrm{s},2}C_5} \end{cases} \tag{10}$$

Consequently, the output voltage induced by the second component is denoted by $U_{\mathrm{O},2}$ and can be derived as

$$U_{\mathrm{O},2} = |U_{\mathrm{O},2}| = \frac{|U_{L,2}|M_{\mathrm{P2S}}}{L_2}. \tag{11}$$

With Eq. (9) and Eq. (11), the overall output voltage U_OUT can be calculated by

$$U_\mathrm{OUT} = \frac{\pi}{4}\sqrt{(U_{\mathrm{O},1}^2 + U_{\mathrm{O},2}^2)} \tag{12}$$

$$= \frac{\pi U_{L,1}}{4L_1}\sqrt{M_{\mathrm{P1S}}^2 + \lambda^2 M_{\mathrm{P2S}}^2}, \tag{13}$$

where $\lambda = L_1 U_{L,2}/L_2 U_{L,1}$. It can be observed that the output voltage is subject to M_{P1S}^2, M_{P2S}^2, and λ. Since M_{P1S}^2 and M_{P2S}^2 have inverse trends with the misalignment, by simply adjusting λ via parameter design, a nearly constant voltage output can be achieved regardless of the misalignment and the load condition.

Δ can be defined to indicate the influence of misalignment, as given by

$$\Delta = M_{\mathrm{P1S}}^2 + \lambda^2 M_{\mathrm{P2S}}^2, \tag{14}$$

The fluctuation of Δ over the whole misalignment range is given by

$$\alpha = \frac{\Delta|_\mathrm{Max} - \Delta|_\mathrm{Min}}{\Delta|_\mathrm{Max} + \Delta|_\mathrm{Min}} \times 100\%, \tag{15}$$

where the $\Delta|_\mathrm{Max}$ and $\Delta|_\mathrm{Min}$ are the maximum and minimum values of Δ versus the misaligment along X-axis, respectively. According to (15) and the measured mutual inductances shown in Fig. 5(a), the plot in Fig. 5(b) illustrates the fluctuation value α versus λ^2. As shown in Fig. 5(b), the minimum value of α is the optimal design point to achieve the best misalignment tolerance capability. Therefore, the value of λ can be determined.

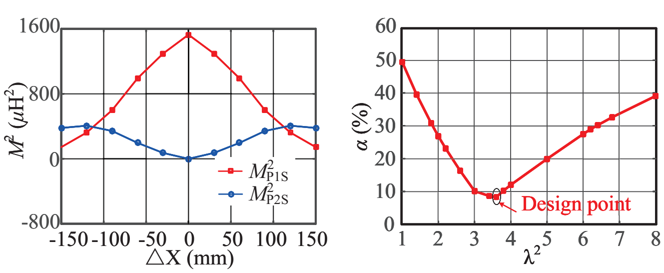

(a) Mutual inductances (b) α versus λ^2

Fig. 5. Mutual inductances and design of λ.

TABLE III
PARAMETERS OF PROPOSED CIRCUIT

Symbol	Definition	Value
C_E	Compensation capacitor in transmitter	28 nF
C_a	Compensation capacitor in transmitter	14.87 μF
C_b	Compensation capacitor in transmitter	40.48 nF
C_2	Compensation capacitor in transmitter	44.62 nF
C_3	Compensation capacitor in transmitter	55.1 nF
C_4	Compensation capacitor in transmitter	5.05 nF
C_c	Compensation capacitor in receiver	38.97 nF
C_d	Compensation capacitor in receiver	21.4 nF
C_5	Compensation capacitor in receiver	25.23 nF
L_E	Compensation inductor in transmitter	44 μH
L_a	Compensation inductor in transmitter	42.59 μH
L_b	Compensation inductor in transmitter	62.57 μH
L_c	Compensation inductor in receiver	65 μH
$L_{\mathrm{P},1}$	The rectangular coil in transmitter	102.74 μH
$L_{\mathrm{P},2}$	The solenoidal coil in transmitter	104.44 μH
L_S	The rectangular coil in receiver	100.405 μH
M_P1S	Mutual inductance ($\Delta\mathrm{X} = 0 - 150$ mm)	39.19-13.385 μH
M_P2S	Mutual inductance ($\Delta\mathrm{X} = 0 - 150$ mm)	0.5-19.17 μH
f_s	Operting frequency	100 kHz
$U_{\mathrm{L},1}$	Calculated amplitude of fundamental harmonic	193.1 V
$U_{\mathrm{L},2}$	Calculated amplitude of fundamental harmonic	129 V
U_DC	Input DC voltage	110 V
U_OUT	Output DC voltage	96 V
D	Duty cycle	0.5
D_Z	ZVS margin	0.11

IV. Experimental Validation

To validate the proposed method, a prototype of the single-switch IPT system is built as shown in Fig. 6. This prototype includes a DC input, a transmitter circuit, a loosely coupled transformer, a receiver circuit, and an electronics load. Only a single power switch is used in the proposed system. The key parameters are summarized in Table III.

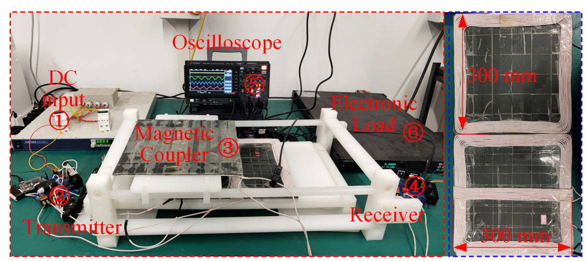

Fig. 6. Photograph of the proposed circuit.

Fig. 7 illustrates the current waveforms of the proposed circuit under both aligned and maximum misalignment conditions of the coils. The corresponding current values are presented in Fig. 7(a) and (b).

As shown in Fig. 7(c) and (d), the Fourier decomposition results of the coil current in Fig. 7(a) and (b) demonstrate that the second harmonic effectively contributes to power replenishment during coil misalignment.

Fig. 8(a) characterizes the output voltage variation with respect to displacement. Throughout the studied misalignment range, the output voltage of the proposed circuit maintains relative stability, demonstrating the correctness of the proposed method. Fig. 8(b) quantifies the DC-to-DC conversion efficiency under various misalignment conditions. The system efficiency reaches approximately 90.02 % under alignment and

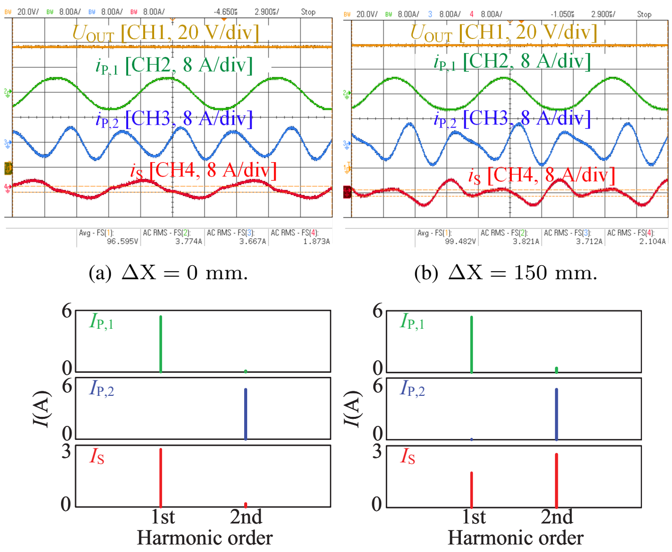

(a) $\Delta X = 0$ mm. (b) $\Delta X = 150$ mm.

(c) $\Delta X = 0$ mm (d) $\Delta X = 150$ mm

Fig. 7. Operating waveforms of the transmitter coil currents i_{P1}, i_{P2}, and i_S and their Fourier analysis.

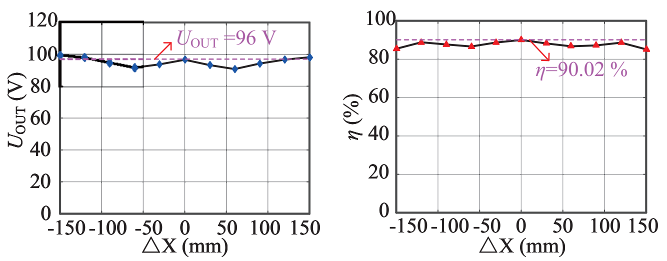

(a) Output voltage (b) Power efficiency

Fig. 8. Measured output voltage and power efficiency against misalignment.

maintains above 85 % throughout the studied misalignment range.

V. Conclusion

This letter proposes a single-switch IPT circuit utilizing the fundamental and second harmonics to drive the unipolar-bipolar composite coils for misalignment tolerance. One coil is excited by the fundamental harmonic as usual, while the other is driven by extracting the significant inherent second harmonic from the single-switch IPT driver, eliminating the need for additional inverters. The proposed method is detailed with compensation design methodology and experimentally validated with a rectangular solenoidal pad. Compared with conventional methods, the proposed method reduces circuit complexity by requiring only a single power switch and simplifies control, as no active detection and control are needed.

References

[1] V. B. Vu, A. Ramezani, and A. Trivino, "Operation of inductive charging systems under misalignment conditions: a review for electric vehicles," *IEEE Trans. Transport. Electrific.,* vol. 9, no. 1, pp. 1857–1887, Mar. 2023.

[2] S. Jayalath and A. Khan, "Design, challenges, and trends of inductive power transfer couplers for electric vehicles: a review," *IEEE J. Emerg. Sel. Topics Ind. Electron.,* vol. 9, no. 5, pp. 6196–6218, Oct. 2021.

[3] A. Sagar, A. Kashyap, and M. A. Nasab, "A comprehensive review of the recent development of wireless power transfer technologies for electric vehicle charging systems," *IEEE Access,* vol. 11, pp. 83703–83751, 2023.

[4] M. Budhia, J. T. Boys, G. A. Covic, C. Y. Huang, "Development of a single-sided flux magnetic coupler for electric vehicle IPT charging systems," *IEEE Trans. Ind. Electron.,* vol. 60, no. 1, pp. 318–328, Jan. 2013.

[5] H. Li, M. Liu, L. Kong, and Y. Wang, "An independent dual-coil driving topology for wireless power transfer," *IEEE Trans. Power Electron.,* vol. 38, no. 2, pp. 1378–1383, Feb. 2023.

[6] H. Xu, Z. Huang, X. L. Li, and C. K. Tse, "Control-free inductive-power-transfer transmitter with misalignment tolerance," *IEEE Trans. Transport. Electrific.,* Accepted, doi: 10.1109/TTE.2025.3560483.

[7] H. Jo, J. A. Lee, D. H. Sim, W. J. Son, and B. K. Lee, "Magnetic characteristics-based selective driving algorithm of IPT EV systems with DDQ power pad for high-efficiency operation and wide misalignment tolerance," in Proc. *IEEE 11th Int. Conf. Power Electron. ECCE Asia,* May 2023, pp. 1031–1037.

[8] Y. Lim and J. Park, "A novel phase-control-based energy beamforming techniques in nonradiative wireless power transfer," *IEEE Trans. Power Electron.,* vol. 30, no. 11, pp. 6274–6287, Nov. 2015.

[9] H. Xu, J. Wang, and Z. Huang, "Large-spacing segmented transmitter track for dynamic wireless power transfer with low output fluctuation," *IEEE Trans. Power Electron.,* vol. 40, no. 9, pp. 14134–14145, Sep. 2025.

[10] H. Xu and Z. Huang, "Alternately arranged segmented transmitter pads with magnetic field complementation for suppressing power fluctuation in dynamic wireless power transfer," *IEEE Trans. Power Electron.,* vol. 39, no. 10, pp. 14091–14102, Oct. 2024.

[11] H. Li, Z. Liu, B. Pan, and Y. Wang, "A wireless power transfer system with high misalignment tolerance and low component count," *IEEE Trans. Power Electron.,* vol. 39, no. 3, pp. 3774–3786, Mar. 2024.

[12] J. Wang, Z. Huang, and X. L. Li, "A dual-frequency resonant single-ended IPT converter with enhanced power transfer capability," *IEEE Trans. Ind. Electron.,* vol. 72, no. 8, pp. 7964–7973, Aug. 2025.

[13] Z. Guo, C. Wang, S. Lin, L. Yang, and X. Lu, "Multiparallel and flexible expansion of single-switch WPT inverter by magnetic integration," *IEEE Trans. Power Electron.,* vol. 38, no. 3, pp. 4167–4180, Mar. 2023.